

Non-equilibrium dynamics of symmetry-resolved entanglement and entanglement asymmetry: Exact asymptotics in Rule 54

Katja Klobas

School of Physics and Astronomy, University of Birmingham, Edgbaston, Birmingham, B15 2TT, UK

E-mail: k.klobas@bham.ac.uk

July 2024

Abstract. Symmetry resolved entanglement and entanglement asymmetry are two measures of quantum correlations sensitive to symmetries of the system. Here we discuss their non-equilibrium dynamics in the Rule 54 cellular automaton, a simple, yet interacting, integrable model. Both quantities can be expressed in terms of the more analytically tractable “charged moments”, i.e. traces of powers of a suitably deformed density matrix, via a replica trick. We express them in terms of a tensor network, which we contract in space using a system of local algebraic relations. This gives the asymptotic form for the charged moments, valid in the regime of large but finite time that is shorter than all the relevant subsystem sizes. In this regime the charge moments decay exponentially with the rate given by the leading solution to a cubic equation.

This paper is dedicated to the memory of Marko Medenjak (1990–2022). In the two years that we overlapped as PhD students and shared the office, he made a deep impact on me in my formative years as a researcher. I have very fond memories of long coffee breaks, during which we finished all the leftover seminar biscuits, and heated physics discussions that led to many scientific bets resulting in free pizza for the whole group. Marko has taught me many useful skills, perhaps the most notable being how to most efficiently roll on the chair from the desk to the whiteboard. He was one of the brightest people I have met, and had a long and successful career ahead of him when he tragically passed away. He will be sorely missed.

1. Introduction

The dynamics of entanglement in non-equilibrium quantum many-body systems show remarkable universality. For instance, after a quantum quench [1, 2] the entanglement entropy between a subsystem and the rest typically shows linear growth followed by saturation at a value extensive in the subsystem size. This happens under very mild conditions, and can be observed in a variety of systems, ranging from integrable [1, 3–6]

to chaotic [7–16]. The reason for this ubiquity of entanglement growth is intimately connected to thermalisation: a quantum system equilibrates after the entanglement has spread through the system, and the entanglement entropy has saturated at a value that coincides with the thermal entropy of the reduced density matrix. The latter is typically extensive regardless of the number of (local) conservation laws, and therefore the same general dependence can emerge for both integrable and chaotic dynamics.

The standard measure of (bipartite) entanglement is the entanglement entropy, but there are many other measures of quantum correlations [17, 18]. Here we consider two examples that probe the interplay between entanglement and symmetries (local conserved charges) of the system. The first one is the *symmetry resolved entanglement entropy* [19–23], defined as the entanglement entropy of a symmetric state reduced to a given symmetry sector. The second one is the *entanglement asymmetry* [24], given by the relative entropy between a non-symmetric state and its symmetrised counterpart. Recently, these quantities have been extensively studied, both theoretically [19–35], and experimentally [36–41]. One of their appealing features for theoretical investigation is the fact that they can be — through a replica trick — recast in terms of so-called *charged moments* (see Sec. 2 for precise definition), which are particularly convenient for analytical manipulations. Despite that, the vast majority of exact results come from free theories, as the exact non-equilibrium dynamics of interacting systems is beyond the reach of existing methods. Refs. [29, 30] proposed an effective description for the dynamics of charged moments in interacting integrable systems. It is based on the idea of exchanging the roles of space and time [42], which maps the non-equilibrium dynamics of charged moments to a stationary quantity accessible through standard tools [43, 44]. Even though this approach has quantitative predictive power, it is hard to rigorously prove it in full generality, and one has to test its predictions against exact results. Here we provide an example where such exact results can be found in closed analytical form.

Specifically, we consider the reversible cellular automaton Rule 54 [45], which is a model on a discrete lattice of qubits with time-evolution defined in discrete time. In recent years this model has been recognised as an example of interacting integrable model [46, 47], whose simplicity allows for exact characterization of various non-equilibrium properties [48–57] (see also a review [58]). The main technical tool we use here is a generalization of the techniques introduced in Refs. [59–61], which are based on space-time-duality ideas [42, 62–71]. In essence, one first recasts the charged moments as a tensor network, and then contracts it in the *space* direction, which can be done exactly due to a set of local algebraic relations fulfilled by the model. This procedure gives access to the charged moments for short times, that is, times smaller than the sizes of all the subsystems, reproducing the results of Refs. [29, 30].

The rest of the paper is organized as follows. In Sec. 2 we present the precise definitions of the quantities of interest. In Sec. 3, we specialise them to the system and quench protocol considered, and express them in terms of a transfer matrix implementing the evolution in space. In Sec. 4 we characterise the fixed points of this transfer matrix, which encode all the information on the short-time regime. The fixed points are then

used in Sec. 5 to work out the asymptotic form of charged moments. Finally, Sec. 6 contains our closing remarks. Some of the technical steps are relegated to the two appendices.

2. The quantities of interest

We assume quantum quench protocol: initially a closed quantum system is prepared in a state $|\Psi_0\rangle$, and then it is left to evolve unitarily so that at time t the system is described by a pure state $|\Psi_t\rangle$. We wish to characterize correlations and fluctuations of conserved charges in the system, which we will capture by the *charged moments* $Z_{\alpha,\beta}(t)$, defined with respect to an extensive conserved charge Q ,

$$Q = \sum_j q_j, \quad q_j = \mathbb{1}^{\otimes j-1} \otimes q \otimes \mathbb{1}^{\otimes L-j-r+1} \quad (2.1)$$

where q is a local operator that acts nontrivially on r consecutive sites[‡]. Using Q , we define the charged moments as

$$Z_{\alpha,\beta}(t) = \text{tr}[e^{i\beta_1 Q_A} \rho_A(t) e^{i\beta_2 Q_A} \rho_A(t) \cdots e^{i\beta_\alpha Q_A} \rho_A(t)], \quad \beta = [\beta_1 \quad \beta_2 \quad \cdots \quad \beta_\alpha], \quad (2.2)$$

where $\alpha \in \mathbb{N}$ is analogous to the Rényi index, $\beta \in \mathbb{C}^\alpha$, and $\rho_A(t)$, Q_A are the state and charge reduced to a subsystem A ,

$$\rho_A(t) = \text{tr}_{\bar{A}} |\Psi_t\rangle\langle\Psi_t|, \quad Q_A = \sum_{\substack{j \\ [j,j+r-1] \subseteq A}} q_j. \quad (2.3)$$

Charged moments contain information about how correlations are shared between the subsystem A and the complement \bar{A} . For instance, in the limit $\beta \rightarrow \mathbf{0}$, one recovers Rényi entanglement entropies,

$$S_A^{(\alpha)}(t) = \frac{1}{1-\alpha} \text{tr}[\rho_A^\alpha(t)] = \frac{1}{1-\alpha} Z_{\alpha,\mathbf{0}}(t). \quad (2.4)$$

Another special point is $\alpha \rightarrow 1$, $\beta \rightarrow \beta$, in which case the charged moments reduce to the *full counting statistics*,

$$Z_{1,\beta}(t) = \text{tr}[e^{\beta Q_A} \rho_A(t)]. \quad (2.5)$$

For $\alpha > 1$, and generic β , the charged moments themselves do not immediately reduce to known quantities, but they can be related to Rényi entanglement entropies of the state reduced to different symmetry sectors. To see this, let us first consider a case when the initial state $|\Psi_0\rangle$ is an eigenstate of the charge, which means that at time t the state $|\Psi_t\rangle\langle\Psi_t|$ commutes with Q . Then we define $\rho_{A,q}(t)$ as the reduced state projected to the subspace with the value of charge equal to q ,

$$\rho_{A,q}(t) = \Pi_q \rho_A(t) \Pi_q = \Pi_q \rho_A(t), \quad \Pi_q = \frac{1}{2\pi} \int_{-\pi}^{\pi} d\beta e^{i\beta(Q_A - q)}, \quad (2.6)$$

[‡] In the general discussion we will always assume $r = 1$, as we implicitly rely on $Q = Q_A \oplus Q_{\bar{A}}$. If $r > 1$ this does not hold anymore, but the corrections are subleading in the sizes of subsystems and time t , therefore most of the discussion carries over to finite r .

where in the Fourier decomposition of the projector Π_q , we implicitly assumed Q to have an integer spectrum, and $q \in \mathbb{Z}$. We denote by $S_{A,q}^{(\alpha)}(t)$ the n -Rényi entropy of $\rho_{A,q}$,

$$S_{A,q}^{(\alpha)}(t) = \frac{1}{1-\alpha} \text{tr}[\rho_{A,q}^\alpha(t)], \quad (2.7)$$

which is referred to as *symmetry resolved Rényi entanglement entropy* [19–23]. Using the above expression for the projector Π_q , we can express it in terms of charged moments as \S

$$\text{tr}[\rho_{A,q}^\alpha(t)] = \frac{1}{2\pi} \int_{-\pi}^{\pi} d\beta Z_{\alpha,[\beta 00\dots 0]}(t). \quad (2.8)$$

On the other hand, if the initial state is *not* an eigenstate of the charge, an interesting question is how quickly does the reduced density matrix become block-diagonal in the charge-eigenstate basis. This is measured by the *entanglement asymmetry* [24], $\Delta S_A(t)$, which is defined as the relative entropy between the reduced density matrix at time t , $\rho_A(t)$, and its symmetrized counterpart, $\bar{\rho}_A(t)$,

$$\Delta S_A(t) = -\text{tr}[\rho_A(t)(\log \bar{\rho}_A(t) - \log \rho_A(t))], \quad (2.9)$$

with

$$\bar{\rho}_A(t) = \sum_{q \in \mathbb{Z}} \Pi_q \rho_A(t) \Pi_q. \quad (2.10)$$

The asymmetry can be conveniently expressed as a $\alpha \rightarrow 1$ limit of the Rényi entanglement asymmetry

$$\Delta S_A(t) = \lim_{\alpha \rightarrow 1} \Delta S^{(\alpha)}(t), \quad \Delta S^{(\alpha)}(t) = \frac{1}{1-\alpha} \log \frac{\text{tr}[\bar{\rho}_A^\alpha(t)]}{\text{tr}[\rho_A^\alpha(t)]}, \quad (2.11)$$

which can in turn be expressed in terms of the charged moments by using the Fourier representation of the projector Π_q (cf. (2.6)),

$$\text{tr}[\bar{\rho}_A^\alpha(t)] = \int_{-\pi}^{\pi} \frac{d\beta_1 d\beta_2 \cdots d\beta_\alpha}{(2\pi)^\alpha} Z_{\alpha,\beta}(t) \delta(\beta_1 + \beta_2 + \dots + \beta_\alpha). \quad (2.12)$$

Note that for a charge symmetric initial state, we have $Z_{\alpha,\beta}(t) = Z_{\alpha,0}(t)$, and therefore $\Delta S^{(\alpha)}(t) = 0$.

3. The setup

3.1. The definition of the dynamics

The dynamics is defined on a system of $2L$ qubits, with the time-evolution defined in two discrete time-steps, so that at time t the state of the system is given as

$$|\Psi_t\rangle = (\mathbb{U}_o \mathbb{U}_e)^t |\Psi_0\rangle, \quad \mathbb{U}_e = \prod_j U_{2j}, \quad \mathbb{U}_o = \prod_j U_{2j-1}. \quad (3.1)$$

\S The initial state commutes with Q , therefore in the leading order also $\rho_A(t)$ commutes with Q_A , and $Z_{\alpha,\beta}(t)$ is the same for all β with the same sum $\sum_{j=1}^\alpha \beta_j$.

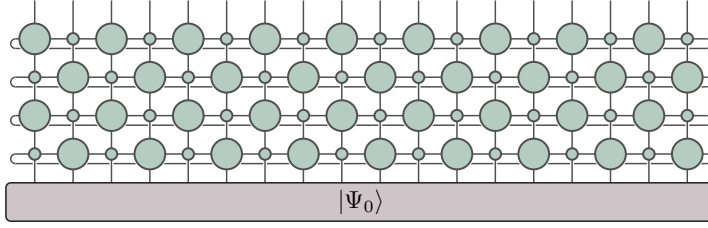


Figure 1. Graphical representation of a time-evolved state $|\Psi_t\rangle$ under the dynamics given by Eq. (3.1) for $L = 9$, and $t = 2$.

Here, U_j is an operator that acts as U to the three sites centred around j ,

$$U_j = \mathbb{1}^{\otimes j-2} \otimes U \otimes \mathbb{1}^{\otimes 2L-j-1}, \quad (3.2)$$

and U is a 3-site local unitary operator given by the following computational-basis matrix elements,

$$\begin{aligned} \langle s'_1 s'_2 s'_3 | U | s_1 s_2 s_3 \rangle &= \delta_{s'_1, s_1} \delta_{s'_2, \chi(s_1, s_2, s_3)} \delta_{s'_3, s_3}, \\ \chi(s_1, s_2, s_3) &\equiv s_1 + s_2 + s_3 + s_1 s_3 \pmod{2}. \end{aligned} \quad (3.3)$$

The operator U deterministically changes the middle site depending on the full 3-site configuration, while the left and right sites are left unchanged. This implies that all the terms in $\mathbb{U}_{e/o}$ mutually commute and can be applied at the same time. The time-evolution can therefore be naturally given in terms of the staggered tensor network pictured in Figure 1, where the two circles represent two distinct tensors defined as

$$\begin{array}{ccc} \begin{array}{c} s_4 \\ \text{---} \\ s_1 \text{---} s_3 \\ \text{---} \\ s_2 \end{array} & = \delta_{s_1, s_2} \delta_{s_2, s_3} \delta_{s_3, s_4}, & \begin{array}{c} s_4 \\ \text{---} \\ s_1 \text{---} \text{---} \\ \text{---} \\ s_2 \end{array} = \delta_{s_4, \chi(s_1, s_2, s_3)}. \end{array} \quad (3.4)$$

3.2. The simplest conserved charges

The model is integrable [46, 47] and exhibits an infinite number of conservation laws. Here we will consider the two conserved quantities with the shortest support, $Q^{(+)} = \sum_j q_j^+$, and $Q^{(-)} = \sum_j q_j^-$,

$$q_j^{(+)} = \frac{1 - \sigma_{j+1}^z}{4} (2 + \sigma_{j+2}^z + \sigma_j^z \sigma_{j+2}^z), \quad q_j^{(-)} = \frac{(-1)^j}{4} (1 + \sigma_j^z \sigma_{j+1}^z - \sigma_j^z - \sigma_{j+1}^z), \quad (3.5)$$

which can be interpreted as the total number of particles, and their current respectively. The support of the two operators is larger than 1, which implies that the object $e^{i\beta Q_A^\pm}$ (where A is a finite subsystem) is not in a product form (contrary to $U(1)$ charges considered in [29]). However, their finite support implies an efficient MPO representation with a finite bond dimension. In particular, in the case of $Q^{(-)}$, the auxiliary space is two-dimensional, and the MPO has the following staggered structure,

$$e^{i\beta Q_A^-} = \text{[staggered MPO structure]}, \quad (3.6)$$

where the vertical legs represent 1-qubit physical degrees of freedom, while the two sets of matrices are

$$\begin{array}{c} s \\ \hbox{\scriptsize \sf wedge} \\ b \end{array} = \delta_{s,0} \delta_{b,0} \begin{bmatrix} 1 & 0 \\ 1 & 0 \end{bmatrix} + \delta_{s,1} \delta_{b,1} \begin{bmatrix} 0 & 1 \\ 0 & e^{i\beta} \end{bmatrix}, \quad \quad \begin{array}{c} s \\ \hbox{\scriptsize \sf wedge} \\ b \end{array} = \begin{array}{c} s \\ \hbox{\scriptsize \sf wedge} \\ b \end{array} \Big|_{\beta \leftrightarrow -\beta}, \quad (3.7)$$

and the boundary vectors in the auxiliary space are chosen as

$$\mathbb{H} = \begin{bmatrix} 1 \\ 0 \end{bmatrix}^T, \quad \mathbb{H} = \begin{bmatrix} 1 \\ 1 \end{bmatrix}. \quad (3.8)$$

Similarly, $e^{i\beta Q^{(+)}}$ can be also represented as an MPO, but the larger support implies a larger bond dimension (in particular, it is 3), and there is no even-odd staggering effect,

$$e^{i\beta Q_A^+} = \parallel \downarrow \quad \downarrow \quad \downarrow \quad \downarrow \quad \downarrow \quad \downarrow \parallel, \quad (3.9)$$

with

$$\begin{array}{c} s \\ \diagdown \\ \text{---} \\ \diagup \\ b \end{array} = \delta_{s,0} \delta_{b,0} \begin{bmatrix} 1 & 0 & 0 \\ e^{2i\beta} & 0 & 0 \\ 1 & 0 & 0 \end{bmatrix} + \delta_{s,1} \delta_{b,1} \begin{bmatrix} 0 & 1 & 0 \\ 0 & 0 & e^{i\beta} \\ 0 & 0 & e^{i\beta} \end{bmatrix}, \quad \mathbb{I} = \begin{bmatrix} 0 \\ \frac{e^{-i\beta}}{1+e^{i\beta}} \\ \frac{1}{1+e^{i\beta}} \end{bmatrix}^T, \quad \mathbb{I} = \begin{bmatrix} 1 \\ 1 \\ e^{-i\beta} \end{bmatrix}. \quad (3.10)$$

Note that for simplicity we use the same notation for the auxiliary degrees of freedom and boundary vectors in the two cases, but it is always clear from the context which one is used.

3.3. Initial states

The reduced density matrix $\rho_A(t)$ is the state $\rho(t) = |\Psi_t\rangle\langle\Psi_t|$ reduced to the subsystem A , where the initial state $|\Psi_0\rangle$ is chosen to be from the family of *solvable* initial states introduced in [59, 60],

$$|\Psi_0\rangle = (|\psi_1\rangle \otimes |\psi_2\rangle)^{\otimes L}, \quad |\psi_1\rangle = \begin{bmatrix} 1 \\ 0 \end{bmatrix}, \quad |\psi_2\rangle = \begin{bmatrix} \sqrt{1-\vartheta} \\ \sqrt{\vartheta} \end{bmatrix}, \quad 0 < \vartheta < 1. \quad (3.11)$$

After being initialized in one of these states, the system can be shown [60] to relax to the family of Gibbs states determined by the first one of the conserved quantities introduced above, $\rho \sim e^{\mu Q^{(+)}}$, with the chemical potential $\mu = \log(\vartheta^{-1} - 1)$.

3.4. Space evolution

The definitions above completely specify our setup, and by denoting the Hermitian conjugates of time-evolution tensors (3.4) with red, \parallel

$$\begin{array}{c} \text{---} \\ | \end{array} \text{---} \textcolor{red}{\bullet} = \begin{array}{c} \text{---} \\ | \end{array} \text{---} \textcolor{teal}{\bullet}^\dagger, \quad \begin{array}{c} \text{---} \\ | \end{array} \text{---} \textcolor{red}{\circ} = \begin{array}{c} \text{---} \\ | \end{array} \text{---} \textcolor{teal}{\circ}^\dagger, \quad (3.12)$$

we are able to represent e.g. $Z_{1,\beta}^{(+)}(l,t)$ as shown in Fig. 2. The graphical representation of the tensor network suggests that $Z_{1,\beta}^{(+)}$ can be equivalently contracted in *space* rather

|| We note that in our case the red and green tensors are the same, as the model is left-right symmetric, deterministic, and reversible. However, the formulation with two different colours naturally generalises to a more general setting, therefore we decided to keep the distinction between the two sets of tensors.

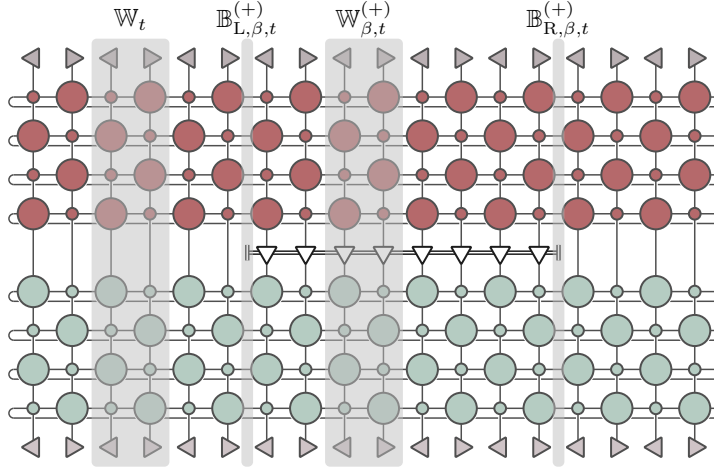


Figure 2. The diagrammatic representation of $Z_{1,\beta}^+(l,t)$ for $L = 9$, $l = 4$, and $t = 2$. The shaded boxes highlight the objects appearing in Eq. (3.16).

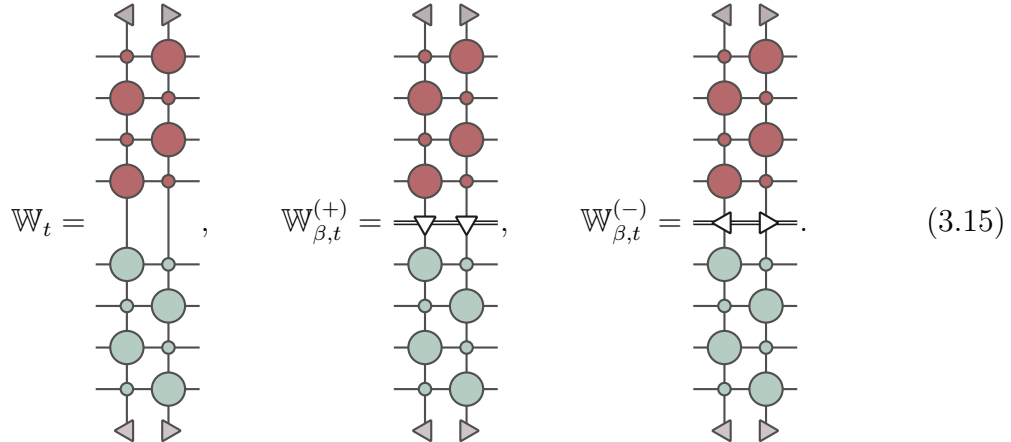
than in time. In particular, we introduce Hilbert space of the *temporal chain* of $2t$ qubits,

$$\mathcal{V}_t = (\mathbb{C}^2)^{\otimes 2t}, \quad (3.13)$$

and define transfer matrices \mathbb{W}_t , $\mathbb{W}_{\beta,t}^{(\pm)}$ that act on $2 \times 2t$ vertical lattice sites, and (possibly) the auxiliary degree of freedom,

$$\mathbb{W}_t \in \text{End}(\mathcal{V}_t \otimes \mathcal{V}_t), \quad \mathbb{W}_{\beta,t}^{(+)} \in \text{End}(\mathcal{V}_t \otimes \mathbb{C}^3 \otimes \mathcal{V}_t), \quad \mathbb{W}_{\beta,t}^{(-)} \in \text{End}(\mathcal{V}_t \otimes \mathbb{C}^2 \otimes \mathcal{V}_t). \quad (3.14)$$

In particular, space transfer matrices are built by two consecutive rows of the diagram in Fig. 2 (and an analogous one corresponding to $Z_{1,\beta}^{(-)}(l,t)$),



In terms of these transfer matrices the moments $Z_{1,\beta}^{(\pm)}(l,t)$ take the following form,

$$Z_{1,\beta}^{(\pm)}(l,t) = \text{tr} \left[\mathbb{W}_t^{L-l} \mathbb{B}_{L,\beta,t}^{(\pm)} \mathbb{W}_{\beta,t}^{(\pm)} \mathbb{B}_{R,\beta,t}^{(\pm)} \right], \quad (3.16)$$

where $\mathbb{B}_{L/R,\beta,t}^{(\pm)}$ act as identity on both \mathbb{V}_t , and as boundary vectors \Rightarrow , \Leftarrow on the auxiliary degree of freedom (see Fig. 2).

More complicated charged moments $Z_{\alpha,\beta}^{(\pm)}(l, t)$ are obtained by considering α copies of transfer matrices that are connected in a staggered way,

$$Z_{\alpha,\beta}^{(\pm)}(l, t) = \text{tr} \left[\mathbb{P}_{\alpha,t}^\dagger \left(\mathbb{W}_t^{\otimes \alpha} \right)^{L-l} \mathbb{P}_{\alpha,t} \mathbb{B}_{L,\alpha,\beta,t}^{(\pm)} \left(\mathbb{W}_{\beta_1,t}^{(\pm)} \otimes \mathbb{W}_{\beta_2,t}^{(\pm)} \otimes \cdots \otimes \mathbb{W}_{\beta_\alpha,t}^{(\pm)} \right)^l \mathbb{B}_{R,\alpha,\beta,t}^{(\pm)} \right], \quad (3.17)$$

where $\mathbb{B}_{L/R,\alpha,\beta,t}^{(\pm)}$ is the multi-copy generalization of $\mathbb{B}_{L/R,\beta,t}^{(\pm)}$,

$$\mathbb{B}_{L/R,\alpha,\beta,t}^{(\pm)} = \mathbb{B}_{L/R,\beta_1,t}^{(\pm)} \otimes \mathbb{B}_{L/R,\beta_2,t}^{(\pm)} \otimes \cdots \otimes \mathbb{B}_{L/R,\beta_\alpha,t}^{(\pm)}, \quad (3.18)$$

and $\mathbb{P}_{\alpha,t} \in \text{End}(\mathcal{V}_t^{\otimes 2\alpha})$ is a permutation operator that periodically shifts *even* vectors in a tensor product of 2α states from \mathcal{V}_t ,

$$\mathbb{P}_{\alpha,t} |x_1\rangle \otimes |x_2\rangle \otimes \cdots \otimes |x_{2\alpha}\rangle = |x_1\rangle \otimes |x_{2\alpha}\rangle \otimes |x_3\rangle \otimes |x_2\rangle \otimes \cdots \otimes |x_{2\alpha-2}\rangle. \quad (3.19)$$

4. Fixed-points of the space transfer matrix

The representation of charged moments in terms of space transfer matrices (cf. (3.17)) in general offers no benefit as it is completely equivalent to the definition (2.2). However, the locality and unitarity of time-evolution imply that \mathbb{W}_t has a unique maximal eigenvalue 1, all the other eigenvalues are equal to 0, and the largest Jordan block is of size at most $2t + 1$. Therefore, a high-enough power of \mathbb{W}_t can be substituted by a projector to its *fixed points* (i.e. leading left and right eigenvectors),

$$\mathbb{W}_t |r_t\rangle = |r_t\rangle, \quad \langle l_t| \mathbb{W}_t = \langle l_t|, \quad \mathbb{W}_t^x|_{x>2t+1} = |r_t\rangle\langle l_t|. \quad (4.1)$$

The additional auxiliary degree of freedom due to $e^{i\beta Q_A^{(\pm)}}$ changes the spectral properties of the transfer matrix $\mathbb{W}_{\beta,t}^{(\pm)}$, so that the leading eigenvalue is no longer necessarily 1. Nonetheless, as is shown in [Appendix A](#), the leading eigenvalue $\Lambda_\beta^{(\pm)}$ is t -independent and unique, and a repeated application of the transfer matrix again projects to the leading eigenvectors,

$$\begin{aligned} \mathbb{W}_{\beta,t}^{(\pm)} |r_{\beta,t}^{(\pm)}\rangle &= \Lambda_\beta^{(\pm)} |r_{\beta,t}^{(\pm)}\rangle, & \langle l_{\beta,t}^{(\pm)}| \mathbb{W}_{\beta,t}^{(\pm)} &= \Lambda_\beta^{(\pm)} \langle l_{\beta,t}^{(\pm)}|, \\ \lim_{x \rightarrow \infty} \left(\frac{1}{\Lambda_\beta^{(\pm)}} \mathbb{W}_{\beta,t}^{(\pm)} \right)^x &= \frac{|r_{\beta,t}^{(\pm)}\rangle\langle l_{\beta,t}^{(\pm)}|}{\langle r_{\beta,t}^{(\pm)}|l_{\beta,t}^{(\pm)}\rangle}. \end{aligned} \quad (4.2)$$

Therefore in the regime of large system and subsystem sizes (compared to t) the behaviour of charged moments $Z_{\alpha,\beta}^{(\pm)}(l, t)$ is completely determined by the properties of leading eigenvalues $\Lambda_\beta^{(\pm)}$, and the corresponding eigenvectors $|r_{\beta,t}^{(\pm)}\rangle$, $\langle l_{\beta,t}^{(\pm)}|$, $|r_t\rangle$, $\langle l_t|$.

4.1. Fixed points of \mathbb{W}_t

We start by summarizing the construction of the fixed points of \mathbb{W}_t , which was introduced in Refs. [\[59, 60\]](#). The fixed points can be conveniently expressed in the

following MPO form,

$$\langle l_t | = \begin{array}{c} \text{[vertical lines]} \\ | \end{array} \quad | r_t \rangle = \begin{array}{c} \text{[vertical lines]} \\ | \end{array} \quad (4.3)$$

where the ticked vertical line represents the auxiliary vector space. It is straightforward to see that the ansatz for $\langle l_t |$ gives the left fixed point of the transfer matrix, if the following set of algebraic relations is fulfilled,

$$\begin{array}{c} \text{[vertical lines]} \\ | \end{array} = \begin{array}{c} \text{[vertical lines]} \\ | \end{array}, \quad \begin{array}{c} \text{[vertical lines]} \\ | \end{array} = \begin{array}{c} \text{[vertical lines]} \\ | \end{array}, \quad \begin{array}{c} \text{[vertical lines]} \\ | \end{array} = \begin{array}{c} \text{[vertical lines]} \\ | \end{array}, \quad (4.4)$$

$$\begin{array}{c} \text{[vertical lines]} \\ | \end{array} = \begin{array}{c} \text{[vertical lines]} \\ | \end{array}, \quad \begin{array}{c} \text{[vertical lines]} \\ | \end{array} = \begin{array}{c} \text{[vertical lines]} \\ | \end{array}, \quad (4.5)$$

and an analogous set of left-right flipped relations ensures that $|r_t\rangle$ is the right fixed point. A solution to these relations exists for the 3-dimensional auxiliary vector space [60],

$$\begin{aligned} 0 \leftarrow 0 &= \begin{bmatrix} 1 - \vartheta & 1 - \vartheta & -1 + \vartheta \\ \vartheta & \vartheta & 1 - \vartheta \\ \vartheta & -\frac{\vartheta^2}{1-\vartheta} & -\vartheta \end{bmatrix}, & 1 \leftarrow 1 &= \begin{bmatrix} 0 & 1 & 0 \\ 1 & 0 & 0 \\ 0 & 0 & 0 \end{bmatrix}, \\ 0 \leftarrow 1 &= 1 \leftarrow 0 &= \begin{bmatrix} 0 & 1 - \vartheta & -1 + \vartheta \\ \vartheta & 0 & 0 \\ \vartheta & 0 & 0 \end{bmatrix}, & s \leftarrow b &= \delta_{b,s} \begin{bmatrix} \delta_{s,0} & 0 & 0 \\ 0 & \delta_{s,1} & 0 \\ 0 & 0 & \delta_{s,1} \end{bmatrix}, \end{aligned} \quad (4.6)$$

while the two-step bulk tensor , and the boundary vectors \mathbf{T} , , and , are reported in Appendix B. Here the parameter ϑ is set by the initial state (3.11).

4.2. Leading eigenvectors of generalized transfer matrices

We use the ideas summarized above to find leading eigenvectors of $\mathbb{W}_{\beta,t}^{(\pm)}$. We again assume an MPO representation similar to (4.3),

$$\langle l_{\beta,t}^{(+)} | = \text{[Diagram 1]}, \quad | r_{\beta,t}^{(+)} \rangle = \text{[Diagram 2]}, \quad \langle l_{\beta,t}^{(-)} | = \text{[Diagram 3]}, \quad | r_{\beta,t}^{(-)} \rangle = \text{[Diagram 4]}. \quad (4.7)$$

Note that in the case of $Q^{(+)}$ we assume the left and right eigenvectors to be made up of the same bulk tensors, while for $Q^{(-)}$ they change. This is due to the symmetry of charges: $Q^{(+)}$ is even under left-right reflection, while $Q^{(-)}$ is odd. ¶

To find tensors that constitute fixed points we again assume a set of appropriate local algebraic relations. In particular, the relations fulfilled by the bottom and bulk tensors only (i.e. those given by Eq. (4.4)) stay unchanged, while the ones involving top boundary vectors (cf. Eq. (4.5)) have to be amended to allow for the additional MPO auxiliary space,

$$\text{[Diagram 5]} = \text{[Diagram 6]}, \quad \text{[Diagram 7]} = \Lambda_{\beta}^{(+)}, \quad \text{[Diagram 8]} = \text{[Diagram 9]}, \quad \text{[Diagram 10]} = \Lambda_{\beta}^{(-)}, \quad (4.8)$$

while the corresponding set of relations for the top boundary vectors of *right* fixed points read as

$$\text{[Diagram 11]} = \text{[Diagram 12]}, \quad \text{[Diagram 13]} = \Lambda_{\beta}^{(+)}, \quad \text{[Diagram 14]} = \text{[Diagram 15]}, \quad \text{[Diagram 16]} = \Lambda_{\beta}^{(-)}. \quad (4.9)$$

Combining the relevant equations we obtain a set of algebraic relations involving a finite number of variables. Upon solving these we again find a solution with a 3-dimensional

¶ On the other hand, the top boundary vectors do not share this property: they are generically assumed to be different since the matrices defining the MPO representation of $e^{i\beta Q^{(\pm)}}$ (cf. (3.6) and (3.9)) are not symmetric.

representation, where the bulk tensors are simply related to the original ones (4.6),

$$\begin{array}{c} \text{orange diamond} \\ \text{blue diamond} \end{array} = \begin{array}{c} \text{orange diamond} \\ \text{blue diamond} \end{array} = \begin{array}{c} \text{orange diamond} \\ \text{blue diamond} \end{array} = \begin{array}{c} \text{orange diamond} \\ \text{blue diamond} \end{array}, \quad \begin{array}{c} \text{orange square} \\ \text{blue square} \end{array} = \begin{array}{c} \text{orange square} \\ \text{blue square} \end{array}, \quad \begin{array}{c} \text{orange square} \\ \text{blue square} \end{array} = \begin{array}{c} \text{orange square} \\ \text{blue square} \end{array}, \quad (4.10)$$

where Φ , Ψ , and Ω , are diagonal matrices in the auxiliary space,

$$\Phi = \begin{bmatrix} 1 & 0 & 0 \\ 0 & \gamma & 0 \\ 0 & 0 & \gamma \end{bmatrix}, \quad \Psi = \Phi \Big|_{\gamma \rightarrow e^{-i\beta}}, \quad \Omega = \Phi \Big|_{\gamma \rightarrow e^{i\beta}}, \quad \Omega = \Phi \Big|_{\gamma \rightarrow e^{i\beta} \Lambda_\beta^{(+)}}. \quad (4.11)$$

Note that the bulk tensors in $\langle l_{\beta,t}^{(-)} |$ and $| r_{\beta,t}^{(-)} \rangle$ are related to each other through a flip of sign of β . The remaining tensors and boundary vectors are reported in [Appendix B](#). The corresponding eigenvalues are determined as (see [Appendix A](#)),

$$\log \Lambda_\beta^{(\pm)} = \lim_{L \rightarrow \infty} \frac{1}{L} \log \langle \Psi_0 | e^{i\beta Q^{(\pm)}} | \Psi_0 \rangle, \quad (4.12)$$

and are

$$\Lambda_\beta^{(+)} = 1 - \vartheta + \vartheta e^{2i\beta}, \quad \Lambda_\beta^{(-)} = 1. \quad (4.13)$$

Finally, we note that the fixed points are for convenience *not* normalized, but rather we keep the overlap between the right and left eigenvectors to be

$$\langle l_{\beta,t}^{(+)} | r_{\beta,t}^{(+)} \rangle = \Lambda_\beta^{(+)^{2t}}, \quad \langle l_{\beta,t}^{(-)} | r_{\beta,t}^{(-)} \rangle = 1 = \Lambda_\beta^{(-)^{2t}}. \quad (4.14)$$

See [Appendix B.3](#) for details.

5. Asymptotics of charged moments

When the subsystem size l and the system size L are sufficiently large compared to the time t (in particular, when $l, L > 2t + 1$) the charged moments factorize into the two contributions corresponding to the edges of the subsystem,

$$\lim_{l, L \rightarrow \infty} \frac{Z_{\alpha, \beta}^{(\pm)}(l, t)}{\prod_{j=1}^{\alpha} \Lambda_{\beta_j}^{(\pm)} l} = \frac{z_{\alpha, \beta}^{L(\pm)}(t) z_{\alpha, \beta}^{R(\pm)}(t)}{\prod_{j=1}^{\alpha} \Lambda_{\beta_j}^{(\pm)} 2t}, \quad (5.1)$$

where $z_{\alpha, \beta}^{L/R(\pm)}$ are the contributions given by the (un-normalized) leading eigenvectors,

$$\begin{aligned} z_{\alpha, \beta}^{L(\pm)} &= \langle l_t |^{\otimes \alpha} \mathbb{P}_{\alpha, t} \left(\mathbb{B}_{L, \beta_1, t}^{(\pm)} | r_{\beta_1, t}^{(\pm)} \rangle \otimes \mathbb{B}_{L, \beta_2, t}^{(\pm)} | r_{\beta_2, t}^{(\pm)} \rangle \otimes \cdots \otimes \mathbb{B}_{L, \beta_\alpha, t}^{(\pm)} | r_{\beta_\alpha, t}^{(\pm)} \rangle \right), \\ z_{\alpha, \beta}^{R(\pm)} &= \left(\langle l_{\beta_1, t}^{(\pm)} | \mathbb{B}_{R, \beta_1, t}^{(\pm)} \otimes \langle l_{\beta_2, t}^{(\pm)} | \mathbb{B}_{R, \beta_2, t}^{(\pm)} \otimes \cdots \otimes \langle l_{\beta_\alpha, t}^{(\pm)} | \mathbb{B}_{R, \beta_\alpha, t}^{(\pm)} \right) \mathbb{P}_{\alpha, t}^\dagger | r_t \rangle^{\otimes \alpha}. \end{aligned} \quad (5.2)$$

In terms of the fixed-point tensors, these expressions take form of $2t \times 2\alpha$ tensor networks,

$$z_{\alpha, \beta}^{L(-)}(t) = \begin{array}{c} \text{Diagram of a 2t by 2alpha tensor network with orange diamonds and blue squares, labeled z_alpha, beta^{L(-)}(t).} \\ \beta_1 \quad \cdots \quad \beta_\alpha \end{array}, \quad z_{\alpha, \beta}^{R(-)}(t) = \begin{array}{c} \text{Diagram of a 2t by 2alpha tensor network with orange diamonds and blue squares, labeled z_alpha, beta^{R(-)}(t).} \\ \beta_1 \quad \cdots \quad \beta_\alpha \end{array}, \quad (5.3)$$

where the label under a column denotes the value of β in which the tensors in that column are evaluated. The diagrams representing $z_{\alpha,\beta}^{\text{L/R}(+)}(t)$ are analogous, only the tensors with \langle and \rangle are replaced with the corresponding $+$ tensors.

These tensor networks are hard to contract for finite t , but we are able to characterize their large- t asymptotics. We start by introducing the transfer matrix $\mathcal{T}_{\alpha,\gamma}$, defined as

$$\mathcal{T}_{\alpha,\gamma} := \text{Diagram} \quad (5.4)$$

with generic values of γ_j . All four relevant tensor networks can be reproduced by repeatedly applying $\mathcal{T}_{\alpha,\gamma}$ and appropriately setting bottom and top vectors. Moreover, assuming that $\mathcal{T}_{\alpha,\gamma}$ has a unique leading eigenvalue $\lambda_{\alpha,\gamma}$, the boundary vectors play no role in the asymptotic behaviour of left and right contributions. In this case the asymptotic slopes of the logarithms of $z_{\alpha,\beta}^{\text{L/R}(\pm)}$ are completely determined by the leading eigenvalue of the transfer matrix,

$$s_{\alpha,\beta}^{(+)} := \lim_{t \rightarrow \infty} \frac{\log z_{\alpha,\beta}^{\text{R}(+)}(t)}{t} = \lim_{t \rightarrow \infty} \frac{\log z_{\alpha,\beta}^{\text{L}(+)}(t)}{t} = \log \lambda_{\alpha,\gamma} \Big|_{\gamma_j \rightarrow e^{i\beta_j} \Lambda_{\beta_j}^{(+)}} , \quad (5.5)$$

and similarly

$$s_{\alpha,\beta}^{(-)} := \lim_{t \rightarrow \infty} \frac{\log z_{\alpha,\beta}^{\text{R}(-)}(t)}{t} = \lim_{t \rightarrow \infty} \frac{\log z_{\alpha,-\beta}^{\text{L}(-)}(t)}{t} = \log \lambda_{\alpha,\gamma} \Big|_{\gamma_j \rightarrow e^{-i\beta_j}} . \quad (5.6)$$

Note that the symmetry of $Q^{(-)}$ again implies the flip of the sign of β between the contributions of the left and right boundary.

5.1. Spectrum of the transfer matrix

The spectrum of $\mathcal{T}_{\alpha,\gamma}$ can be found by following and appropriately modifying the approach of Ref. [61]. We first clump together two vertical legs and two horizontal legs into single degrees of freedom,

$$\text{Diagram} =: 2s_1 + s_2 = 2b_1 + b_2 , \quad (5.7)$$

so that the transfer matrix is expressed as ⁺

$$\mathcal{T}_{\alpha,\gamma} = \text{Diagram} \quad (5.8)$$

We then perform a convenient local similarity transformation,

$$\text{Diagram} = \text{Diagram} , \quad \text{Diagram} = P , \quad \text{Diagram} = P^{-1} , \quad (5.9)$$

⁺ Note that we are suppressing the subscripts γ_j to lighten the notation. Everywhere in this section each column is assumed to correspond to a different value of γ_j unless explicitly stated.

with the local matrix P given as,

$$P = \begin{bmatrix} 1 & 0 & 0 & 0 & 0 & 0 & 0 & 0 & 0 \\ 0 & 1 & 1 & 0 & 0 & 0 & 0 & 0 & 0 \\ 0 & 1 & \frac{-\vartheta}{1-\vartheta} & 0 & 0 & 0 & 0 & 0 & 0 \\ 0 & 0 & 0 & 1 & 0 & 0 & 1 & 0 & 0 \\ 0 & 0 & 0 & 0 & 1 & 1 & 0 & 1 & 1 \\ 0 & 0 & 0 & 0 & 1 & \frac{-\vartheta}{1-\vartheta} & 0 & 1 & \frac{-\vartheta}{1-\vartheta} \\ 0 & 0 & 0 & 1 & 0 & 0 & \frac{-\vartheta}{1-\vartheta} & 0 & 0 \\ 0 & 0 & 0 & 0 & \frac{-\vartheta}{1-\vartheta} & \frac{-\vartheta}{1-\vartheta} & 0 & 1 & 1 \\ 0 & 0 & 0 & 0 & \frac{-\vartheta}{1-\vartheta} & \frac{\vartheta^2}{(1-\vartheta)^2} & 0 & 1 & \frac{-\vartheta}{1-\vartheta} \end{bmatrix}. \quad (5.10)$$

This gives us a transformed transfer matrix $\tilde{\mathcal{T}}_{\alpha,\gamma}$ that has the same spectrum as $\mathcal{T}_{\alpha,\gamma}$,

$$\tilde{\mathcal{T}}_{\alpha,\gamma} = \text{Diagram} \quad (5.11)$$

The transformed tensors (5.9) satisfy Lemma 1 from Ref. [61]. Namely, for any integer power $m \geq 1$ the following holds,

$$\begin{array}{ccc} \text{Diagram} & = & \text{Diagram} \\ \begin{array}{c} v_1 \\ \vdots \\ v_m \end{array} & \begin{array}{c} w_1 \\ \vdots \\ w_m \end{array} & \begin{array}{c} v_1 \\ \vdots \\ v_m \end{array} \\ \begin{array}{c} v_2 \\ \vdots \\ v_m \end{array} & \begin{array}{c} w_2 \\ \vdots \\ w_m \end{array} & \begin{array}{c} v_2 \\ \vdots \\ v_m \end{array} \\ \begin{array}{c} v_3 \\ \vdots \\ v_m \end{array} & \begin{array}{c} w_3 \\ \vdots \\ w_m \end{array} & \begin{array}{c} v_3 \\ \vdots \\ v_m \end{array} \\ \begin{array}{c} v_4 \\ \vdots \\ v_m \end{array} & \begin{array}{c} w_4 \\ \vdots \\ w_m \end{array} & \begin{array}{c} v_4 \\ \vdots \\ v_m \end{array} \\ \vdots & \vdots & \vdots \\ \begin{array}{c} v_{m-1} \\ v_m \end{array} & \begin{array}{c} w_{m-1} \\ w_m \end{array} & \begin{array}{c} v_{m-1} \\ v_m \end{array} \\ \begin{array}{c} v_1 \\ v_m \end{array} & \begin{array}{c} w_1 \\ w_m \end{array} & \begin{array}{c} v_1 \\ v_m \end{array} \end{array} \\ = \prod_{j=1}^m \delta_{w_j, v_j} & & \end{array} \quad (5.12)$$

The proof follows from a straightforward modification of the proof given in Ref. [61], and will be not repeated here.

The property (5.12) directly implies that traces of powers of $\tilde{\mathcal{T}}_{\alpha,\gamma}$ (and therefore also $\mathcal{T}_{\alpha,\gamma}$) are given as

$$\text{tr}[\mathcal{T}_{\alpha,\gamma}^m] = \text{tr}[\tilde{\mathcal{T}}_{\alpha,\gamma}^m] = \text{tr}[\tilde{\tau}_{\alpha,\gamma}^m], \quad (5.13)$$

where $\tilde{\tau}_{\alpha,\gamma}$ is a 9×9 matrix given by following matrix elements,

$$[\tilde{\tau}_{\alpha,\gamma}]_{w,v} = \text{Diagram} \quad (5.14)$$

Explicitly, the matrix $\tilde{\tau}_{\alpha,\gamma}$ reads as

$$\tilde{\tau}_{\alpha,\gamma} = \begin{bmatrix} (1-\vartheta)^{2\alpha} & 0 & 0 & 0 & 0 & \Gamma & (1-\vartheta)^\alpha & 0 & \Gamma \\ \vartheta^\alpha(1-\vartheta)^\alpha & 0 & 0 & 0 & 0 & 0 & \vartheta^\alpha & 0 & 0 \\ 0 & 0 & 0 & 0 & \Gamma & 0 & 0 & \Gamma & 0 \\ 0 & \vartheta^\alpha\Gamma & \vartheta^\alpha\Gamma & 0 & 0 & 0 & 0 & 0 & 0 \\ 0 & 0 & 0 & \vartheta^\alpha & 0 & 0 & 0 & 0 & 0 \\ 0 & 0 & 0 & (1-\vartheta)^\alpha & 0 & 0 & 0 & 0 & 0 \\ 0 & (1-\vartheta)^\alpha\Gamma & (1-\vartheta)^\alpha\Gamma & 0 & 0 & 0 & 0 & 0 & 0 \\ \vartheta^{2\alpha} & 0 & 0 & 0 & 0 & 0 & 0 & 0 & 0 \\ \vartheta^\alpha(1-\vartheta)^\alpha & 0 & 0 & 0 & 0 & 0 & 0 & 0 & 0 \end{bmatrix}, \quad (5.15)$$

where Γ is a shorthand notation for the product of γ_j ,

$$\Gamma = \prod_{j=1}^{\alpha} \gamma_j. \quad (5.16)$$

This matrix has three non-zero eigenvalues with algebraic and geometric multiplicities equal to 1,

$$\text{Spect}(\tilde{\tau}_{\alpha,\gamma}) = \{\lambda_{\alpha,\gamma}, \lambda_{\alpha,\gamma}^{(1)}, \lambda_{\alpha,\gamma}^{(2)}, 0\}, \quad (5.17)$$

which are obtained as solutions to the following cubic equation,

$$x^3 = (x(1-\vartheta)^\alpha + \vartheta^\alpha\Gamma)^2. \quad (5.18)$$

Here we use $\lambda_{\alpha,\gamma}$ to denote the leading eigenvalue, and we assume it is *isolated*

$$|\lambda_{\alpha,\gamma}| > |\lambda_{\alpha,\gamma}^{(1)}|, |\lambda_{\alpha,\gamma}^{(2)}|, \quad (5.19)$$

which is not always the case. However, as long as Γ does not take a negative real value, there is a gap between the leading and the largest subleading eigenvalue for any $\vartheta \neq 0, 1$.

6. Conclusions

In this paper we extended the approach of Refs. [60, 61] to study time-evolution of charged moments in Rule 54. We formulated the charged moments of the two simplest charges (the total particle number, and the imbalance between right and left movers) in terms of a space transfer matrix, which can be understood as a deformation of the transfer-matrix capturing the dynamics of local observables. We then found the fixed points of this deformed transfer matrix, which are made of tensors that fulfil a set of local algebraic relations analogous to the non-deformed case. This enabled us to fully characterize the charged moments in the early-time regime. We showed that they decay exponentially with a rate given in terms of a solution of a cubic equation. As was argued in Refs. [29, 30], this is a special case of a more general non-linear equation applying for interacting integrable systems, which can be obtained from an equation for equilibrium charged moments upon flipping the roles of space and time.

This work leaves several open questions. Perhaps the most urgent one is to understand what are the limits of the algebraic approach to characterize space evolution.

As is showed here, the fixed points can be explicitly constructed also when the space transfer matrix is deformed by applying $e^{i\beta Q_A^{(\pm)}}$ at time t , where $Q^{(\pm)}$ are the two simplest charges. The natural next step is to understand for which Q is the deformed transfer matrix of Rule 54 still solvable. Does Q need to be conserved, or can it be a more general operator? More generally, a key question is to find a broader class of systems that admit analogous solutions.

Acknowledgments

I thank Bruno Bertini, Pasquale Calabrese, Mario Collura, and Colin Rylands for collaborations on related topics, and Bruno Bertini for the careful reading of the manuscript. This work was supported by the Leverhulme Trust through the Early Career Fellowship No. ECF-2022-324. I warmly acknowledge the hospitality of the University of Ljubljana where this manuscript was finished.

- [1] Calabrese P and Cardy J 2005 Evolution of entanglement entropy in one-dimensional systems *J. Stat. Mech.: Theory Exp.* **2005** P04010
- [2] Calabrese P and Cardy J 2006 Time dependence of correlation functions following a quantum quench *Phys. Rev. Lett.* **96**(13) 136801
- [3] Fagotti M and Calabrese P 2008 Evolution of entanglement entropy following a quantum quench: Analytic results for the XY chain in a transverse magnetic field *Phys. Rev. A* **78**(1) 010306
- [4] Alba V and Calabrese P 2017 Entanglement and thermodynamics after a quantum quench in integrable systems *Proc. Natl. Acad. Sci. U.S.A.* **114** 7947–7951
- [5] Alba V and Calabrese P 2018 Entanglement dynamics after quantum quenches in generic integrable systems *SciPost Phys.* **4**(3) 17
- [6] Lagnese G, Calabrese P and Piroli L 2022 Entanglement dynamics of thermofield double states in integrable models *J. Phys. A: Math. Theor.* **55** 214003
- [7] Läuchli A M and Kollath C 2008 Spreading of correlations and entanglement after a quench in the one-dimensional Bose–Hubbard model *J. Stat. Mech.: Theory Exp.* **2008** P05018
- [8] Kim H and Huse D A 2013 Ballistic spreading of entanglement in a diffusive nonintegrable system *Phys. Rev. Lett.* **111**(12) 127205
- [9] Liu H and Suh S J 2014 Entanglement tsunami: Universal scaling in holographic thermalization *Phys. Rev. Lett.* **112**(1) 011601
- [10] Asplund C T, Bernamonti A, Galli F and Hartman T 2015 Entanglement scrambling in 2d conformal field theory *J. High Energy Phys.* **2015** 110
- [11] Nahum A, Ruhman J, Vijay S and Haah J 2017 Quantum entanglement growth under random unitary dynamics *Phys. Rev. X* **7**(3) 031016
- [12] Pal R and Lakshminarayan A 2018 Entangling power of time-evolution operators in integrable and nonintegrable many-body systems *Phys. Rev. B* **98**(17) 174304
- [13] Bertini B, Kos P and Prosen T 2019 Entanglement spreading in a minimal model of maximal many-body quantum chaos *Phys. Rev. X* **9** 021033
- [14] Gopalakrishnan S and Lamacraft A 2019 Unitary circuits of finite depth and infinite width from quantum channels *Phys. Rev. B* **100**(6) 064309
- [15] Piroli L, Bertini B, Cirac J I and Prosen T 2020 Exact dynamics in dual-unitary quantum circuits *Phys. Rev. B* **101**(9) 094304
- [16] Zhou T and Nahum A 2020 Entanglement membrane in chaotic many-body systems *Phys. Rev. X* **10**(3) 031066

- [17] Amico L, Fazio R, Osterloh A and Vedral V 2008 Entanglement in many-body systems *Rev. Mod. Phys.* **80**(2) 517–576
- [18] Horodecki R, Horodecki P, Horodecki M and Horodecki K 2009 Quantum entanglement *Rev. Mod. Phys.* **81**(2) 865–942
- [19] Laflorencie N and Rachel S 2014 Spin-resolved entanglement spectroscopy of critical spin chains and luttinger liquids *J. Stat. Mech.: Theory Exp.* **2014** P11013
- [20] Goldstein M and Sela E 2018 Symmetry-resolved entanglement in many-body systems *Phys. Rev. Lett.* **120**(20) 200602
- [21] Xavier J C, Alcaraz F C and Sierra G 2018 Equipartition of the entanglement entropy *Phys. Rev. B* **98**(4) 041106
- [22] Bonsignori R, Ruggiero P and Calabrese P 2019 Symmetry resolved entanglement in free fermionic systems *J. Phys. A: Math. Theor.* **52** 475302
- [23] Murciano S, Di Giulio G and Calabrese P 2020 Entanglement and symmetry resolution in two dimensional free quantum field theories *J. High Energy Phys.* **2020** 1–42
- [24] Ares F, Murciano S and Calabrese P 2023 Entanglement asymmetry as a probe of symmetry breaking *Nat. Commun.* **14** 2036
- [25] Ares F, Murciano S, Vernier E and Calabrese P 2023 Lack of symmetry restoration after a quantum quench: An entanglement asymmetry study *SciPost Phys.* **15** 089
- [26] Capizzi L and Mazzoni M 2023 Entanglement asymmetry in the ordered phase of many-body systems: The Ising field theory *J. High Energy Phys.* **2023** 1–36
- [27] Capizzi L and Vitale V 2024 A universal formula for the entanglement asymmetry of matrix product states *Preprint* [arXiv:2310.01962](https://arxiv.org/abs/2310.01962)
- [28] Khor B J J, Kürkçüoglu D M, Hobbs T J, Perdue G N and Klich I 2023 Confinement and kink entanglement asymmetry on a quantum Ising chain *Preprint* [arXiv:2312.08601](https://arxiv.org/abs/2312.08601)
- [29] Bertini B, Calabrese P, Collura M, Klobas K and Rylands C 2023 Nonequilibrium full counting statistics and symmetry-resolved entanglement from space-time duality *Phys. Rev. Lett.* **131**(14) 140401
- [30] Bertini B, Klobas K, Collura M, Calabrese P and Rylands C 2024 Dynamics of charge fluctuations from asymmetric initial states *Phys. Rev. B* **109** 184312
- [31] Murciano S, Ares F, Klich I and Calabrese P 2024 Entanglement asymmetry and quantum Mpemba effect in the XY spin chain *J. Stat. Mech.: Theory Exp.* **2024** 013103
- [32] Caceffo F, Murciano S and Alba V 2024 Entangled multiplets, asymmetry, and quantum mpemba effect in dissipative systems *J. Stat. Mech.: Theory Exp.* **2024** 063103
- [33] Ferro F, Ares F and Calabrese P 2024 Non-equilibrium entanglement asymmetry for discrete groups: The example of the XY spin chain *J. Stat. Mech.: Theory Exp.* **2024** 023101
- [34] Rylands C, Klobas K, Ares F, Calabrese P, Murciano S and Bertini B 2024 Microscopic origin of the quantum mpemba effect in integrable systems *Phys. Rev. Lett.* **133**(1) 010401
- [35] Chen M and Chen H H 2024 Rényi entanglement asymmetry in (1 + 1)-dimensional conformal field theories *Phys. Rev. D* **109**(6) 065009
- [36] Lukin A, Rispoli M, Schittko R, Tai M E, Kaufman A M, Choi S, Khemani V, Léonard J and Greiner M 2019 Probing entanglement in a many-body localized system *Science* **364** 256–260
- [37] Azses D, Haenel R, Naveh Y, Raussendorf R, Sela E and Dalla Torre E G 2020 Identification of symmetry-protected topological states on noisy quantum computers *Phys. Rev. Lett.* **125**(12) 120502
- [38] Neven A, Carrasco J, Vitale V, Kokail C, Elben A, Dalmonte M, Calabrese P, Zoller P, Vermersch B, Kueng R *et al.* 2021 Symmetry-resolved entanglement detection using partial transpose moments *Npj Quantum Inf.* **7** 1–12
- [39] Vitale V, Elben A, Kueng R, Neven A, Carrasco J, Kraus B, Zoller P, Calabrese P, Vermersch B and Dalmonte M 2022 Symmetry-resolved dynamical purification in synthetic quantum matter *SciPost Phys.* **12** 106
- [40] Rath A, Vitale V, Murciano S, Votto M, Dubail J, Kueng R, Branciard C, Calabrese P and

Vermersch B 2023 Entanglement barrier and its symmetry resolution: Theory and experimental observation *PRX Quantum* **4**(1) 010318

[41] Joshi L K, Franke J, Rath A, Ares F, Murciano S, Kranzl F, Blatt R, Zoller P, Vermersch B, Calabrese P *et al.* 2024 Observing the quantum Mpemba effect in quantum simulations *Phys. Rev. Lett.* **133** 010402

[42] Bertini B, Klobas K, Alba V, Lagnese G and Calabrese P 2022 Growth of Rényi entropies in interacting integrable models and the breakdown of the quasiparticle picture *Phys. Rev. X* **12**(3) 031016

[43] Caux J S 2016 The quench action *J. Stat. Mech.: Theory Exp.* **2016** 064006

[44] Takahashi M 1999 *Thermodynamics of One-Dimensional Solvable Models* (Cambridge University Press)

[45] Bobenko A, Bordemann M, Gunn C and Pinkall U 1993 On two integrable cellular automata *Commun. Math. Phys.* **158** 127–134

[46] Friedman A J, Gopalakrishnan S and Vasseur R 2019 Integrable many-body quantum Floquet-Thouless pumps *Phys. Rev. Lett.* **123**(17) 170603

[47] Gombor T and Pozsgay B 2024 Integrable deformations of superintegrable quantum circuits *SciPost Phys.* **16** 114

[48] Prosen T and Mejía-Monasterio C 2016 Integrability of a deterministic cellular automaton driven by stochastic boundaries *J. Phys. A: Math. Theor.* **49** 185003

[49] Prosen T and Buča B 2017 Exact matrix product decay modes of a boundary driven cellular automaton *J. Phys. A: Math. Theor.* **50** 395002

[50] Inoue A and Takesue S 2018 Two extensions of exact nonequilibrium steady states of a boundary-driven cellular automaton *J. Phys. A: Math. Theor.* **51** 425001

[51] Klobas K, Medenjak M, Prosen T and Vanicat M 2019 Time-dependent matrix product ansatz for interacting reversible dynamics *Commun. Math. Phys.* **371** 651–688

[52] Buča B, Garrahan J P, Prosen T and Vanicat M 2019 Exact large deviation statistics and trajectory phase transition of a deterministic boundary driven cellular automaton *Phys. Rev. E* **100**(2) 020103(R)

[53] Klobas K, Vanicat M, Garrahan J P and Prosen T 2020 Matrix product state of multi-time correlations *J. Phys. A: Math. Theor.* **53** 335001

[54] Klobas K and Prosen T 2020 Space-like dynamics in a reversible cellular automaton *SciPost Phys. Core* **2**(2) 10

[55] Gopalakrishnan S 2018 Operator growth and eigenstate entanglement in an interacting integrable Floquet system *Phys. Rev. B* **98**(6) 060302(R)

[56] Gopalakrishnan S, Huse D A, Khemani V and Vasseur R 2018 Hydrodynamics of operator spreading and quasiparticle diffusion in interacting integrable systems *Phys. Rev. B* **98**(22) 220303(R)

[57] Alba V, Bertini B and Fagotti M 2019 Entanglement evolution and generalised hydrodynamics: Interacting integrable systems *SciPost Phys.* **7**(1) 5

[58] Buča B, Klobas K and Prosen T 2021 Rule 54: Exactly solvable model of nonequilibrium statistical mechanics *J. Stat. Mech.: Theory Exp.* **2021** 074001

[59] Klobas K, Bertini B and Piroli L 2021 Exact thermalization dynamics in the “Rule 54” quantum cellular automaton *Phys. Rev. Lett.* **126**(16) 160602

[60] Klobas K and Bertini B 2021 Exact relaxation to Gibbs and non-equilibrium steady states in the quantum cellular automaton Rule 54 *SciPost Phys.* **11**(6) 106

[61] Klobas K and Bertini B 2021 Entanglement dynamics in Rule 54: Exact results and quasiparticle picture *SciPost Phys.* **11**(6) 107

[62] Bañuls M C, Hastings M B, Verstraete F and Cirac J I 2009 Matrix product states for dynamical simulation of infinite chains *Phys. Rev. Lett.* **102**(24) 240603

[63] Müller-Hermes A, Cirac J I and Bañuls M C 2012 Tensor network techniques for the computation of dynamical observables in one-dimensional quantum spin systems *New J. Phys.* **14** 075003

- [64] Hastings M B and Mahajan R 2015 Connecting entanglement in time and space: Improving the folding algorithm *Phys. Rev. A* **91**(3) 032306
- [65] Bertini B, Kos P and Prosen T 2018 Exact spectral form factor in a minimal model of many-body quantum chaos *Phys. Rev. Lett.* **121**(26) 264101
- [66] Bertini B, Kos P and Prosen T 2019 Exact correlation functions for dual-unitary lattice models in 1 + 1 dimensions *Phys. Rev. Lett.* **123**(21) 210601
- [67] Leroose A, Sonner M and Abanin D A 2021 Influence matrix approach to many-body Floquet dynamics *Phys. Rev. X* **11** 021040
- [68] Leroose A, Sonner M and Abanin D A 2021 Scaling of temporal entanglement in proximity to integrability *Phys. Rev. B* **104** 035137
- [69] Sonner M, Leroose A and Abanin D A 2021 Influence functional of many-body systems: Temporal entanglement and matrix-product state representation *Ann. Physics* **435** 168677
- [70] Ippoliti M and Khemani V 2021 Postselection-free entanglement dynamics via spacetime duality *Phys. Rev. Lett.* **126**(6) 060501
- [71] Bertini B, Klobas K and Lu T C 2022 Entanglement negativity and mutual information after a quantum quench: Exact link from space-time duality *Phys. Rev. Lett.* **129**(14) 140503

Appendix A. Spectral properties of space transfer matrices

To find the spectrum of the space-transfer matrices we first note that by definition we have for any $L \geq 1$

$$\text{tr}[\mathbb{W}_{\beta,t}^{(\pm)L}] = \langle \Psi_t | e^{i\beta Q^{(\pm)}} | \Psi_t \rangle = \langle \Psi_0 | e^{i\beta Q^{(\pm)}} | \Psi_0 \rangle = \text{tr}[\mathbb{W}_{\beta,0}^{(\pm)L}], \quad (\text{A.1})$$

where the r.h.s. corresponds to the system defined on $2L$ sites with periodic boundary conditions, in the second equality we used that $Q^{(\pm)}$ is conserved under time-evolution, and the last equality again follows from the definition of the transfer matrix. Transfer matrices $\mathbb{W}_{\beta,0}^{(\pm)}$ act only on the auxiliary space of the $e^{i\beta Q}$ MPO, and take the following form,

$$\mathbb{W}_{\beta,0}^{(+)} = \begin{array}{c} \text{Diagram of a 2-site transfer matrix with two vertical lines and two horizontal lines, each with a double-headed arrow.} \end{array} = \begin{bmatrix} 1 - \vartheta & \vartheta & 0 \\ e^{2i\beta}(1 - \vartheta) & e^{2i\beta}\vartheta & 0 \\ (1 - \vartheta) & \vartheta & 0 \end{bmatrix}, \quad \mathbb{W}_{\beta,0}^{(-)} = \begin{array}{c} \text{Diagram of a 2-site transfer matrix with two vertical lines and two horizontal lines, each with a single-headed arrow pointing right.} \end{array} = \begin{bmatrix} 1 - \vartheta & \vartheta \\ 1 - \vartheta & \vartheta \end{bmatrix}. \quad (\text{A.2})$$

Both these matrices have exactly one non-zero eigenvalue, which we denote by $\Lambda_{\beta}^{(\pm)}$, and are

$$\Lambda_{\beta}^{(+)} = 1 - \vartheta + e^{2i\beta}\vartheta, \quad \Lambda_{\beta}^{(-)} = 1. \quad (\text{A.3})$$

Note that the matrices $\mathbb{W}_{\beta,0}^{(\pm)}$ have trivial Jordan structure, and therefore

$$\frac{1}{\Lambda_{\beta}^{(\pm)}} \mathbb{W}_{\beta,0}^{(\pm)} = \frac{|r_{\beta,0}^{(\pm)}\rangle\langle l_{\beta,0}^{(\pm)}|}{\langle r_{\beta,0}^{(\pm)}|l_{\beta,0}^{(\pm)}\rangle}. \quad (\text{A.4})$$

This ceases to be the case for $t > 0$, when the Jordan structure of the transfer matrix becomes richer, but using the conservation of $Q^{(\pm)}$ together with locality of time-evolution and (A.4) one can show that we have

$$\left(\frac{1}{\Lambda_{\beta}^{(\pm)}} \mathbb{W}_{\beta,0}^{(\pm)} \right)^x \Big|_{x>2t+1} = \frac{|r_{\beta,0}^{(\pm)}\rangle\langle l_{\beta,0}^{(\pm)}|}{\langle r_{\beta,0}^{(\pm)}|l_{\beta,0}^{(\pm)}\rangle}. \quad (\text{A.5})$$

Appendix B. Fixed-point tensors

Appendix B.1. Auxiliary two-step tensors

Here we report the remaining tensor needed for Eqs. (4.4), (4.8), and (4.9) to hold. The blue tensors take the following form,

$$\begin{aligned}
\begin{array}{c} 0 \\ 0 \end{array} \begin{array}{c} 0 \\ 0 \end{array} &= \begin{bmatrix} (1-\vartheta)^2 & (1-\vartheta)^2 & -(1-\vartheta)^2 \\ (1-\vartheta)\vartheta & (1-\vartheta)\vartheta & -(1-\vartheta)\vartheta \\ (1-\vartheta)\vartheta & -\vartheta^2 & \vartheta^2 \end{bmatrix}, & \begin{array}{c} 1 \\ 0 \end{array} \begin{array}{c} 1 \\ 0 \end{array} &= \begin{bmatrix} \vartheta & 0 & 0 \\ 0 & \vartheta & (1-\vartheta) \\ 0 & 0 & 0 \end{bmatrix}, \\
\begin{array}{c} 0 \\ 0 \end{array} \begin{array}{c} 0 \\ -1 \end{array} &= \begin{bmatrix} 0 & (1-\vartheta)^2 & -(1-\vartheta)^2 \\ 0 & (1-\vartheta)\vartheta & -(1-\vartheta)\vartheta \\ 0 & -\vartheta^2 & \vartheta^2 \end{bmatrix}, & \begin{array}{c} 1 \\ 0 \end{array} \begin{array}{c} 1 \\ -1 \end{array} &= \begin{bmatrix} \vartheta & 0 & 0 \\ 0 & 0 & 0 \\ 0 & 0 & 0 \end{bmatrix}, \\
\begin{array}{c} 0 \\ 1 \end{array} \begin{array}{c} 0 \\ -1 \end{array} &= \begin{bmatrix} 0 & 1-\vartheta & 0 \\ 0 & \vartheta & 0 \\ 0 & 0 & \vartheta \end{bmatrix}, & \begin{array}{c} 1 \\ 1 \end{array} \begin{array}{c} 1 \\ -1 \end{array} &= \begin{bmatrix} \vartheta & 0 & 0 \\ 1-\vartheta & 0 & 0 \\ 0 & 0 & 0 \end{bmatrix}, & (B.1) \\
\begin{array}{c} 0 \\ 0 \end{array} \begin{array}{c} -1 \\ 1 \end{array} &= \begin{bmatrix} 0 & 1-\vartheta & 0 \\ 0 & \vartheta & 0 \\ 0 & 0 & \vartheta \end{bmatrix}, & s \begin{array}{c} -1 \\ b \end{array} &= 0, \\
\begin{array}{c} 0 \\ 1 \end{array} \begin{array}{c} -1 \\ 0 \end{array} &= \begin{bmatrix} 0 & 0 & 0 \\ 0 & \vartheta^2 & (1-\vartheta)\vartheta \\ 0 & \vartheta^2 & (1-\vartheta)\vartheta \end{bmatrix}, & s_1 \begin{array}{c} -b_1 \\ b_1 \end{array} &= b_1 \begin{array}{c} -s_1 \\ b_2 \end{array}, \\
& & s_2 \begin{array}{c} -b_2 \\ b_2 \end{array} &= b_2 \begin{array}{c} -s_2 \\ b_2 \end{array}.
\end{aligned}$$

The orange tensors are very similar, with the majority of the tensors being the same as blue,

$$\begin{array}{c} s_1 \\ s_2 \end{array} \begin{array}{c} b_1 \\ b_2 \end{array} \Big|_{s_1+s_2 < 2} = \begin{array}{c} s_1 \\ s_2 \end{array} \begin{array}{c} b_1 \\ b_2 \end{array}, \quad (B.2)$$

while for $s_1 = s_2 = 1$ one needs to multiply the relevant tensors with a transformation analogous to (4.11)

$$\begin{array}{c} 1 \\ s \end{array} \begin{array}{c} -1 \\ b \end{array} = \begin{array}{c} 1 \\ s \end{array} \begin{array}{c} -1 \\ b \end{array}, \quad \begin{array}{c} \gamma \\ 0 \\ 0 \end{array} = \begin{bmatrix} \gamma & 0 & 0 \\ 0 & 1 & 0 \\ 0 & 0 & 1 \end{bmatrix}, \quad \begin{array}{c} \gamma \\ \gamma \\ \gamma \end{array} = \begin{array}{c} \gamma \\ \gamma \\ \gamma \end{array} = \gamma. \quad (B.3)$$

Note that this holds for any label \langle , \rangle , and $+$ upon replacing γ with $e^{-i\beta}$, $e^{i\beta}$, and $e^{i\beta}\Lambda_\beta^{(+)}$ respectively.

Appendix B.2. Boundary tensors

The bottom boundary tensors are all the same and do not depend on the value of β ,

$$\begin{array}{c} \blacktriangleleft \\ \blacktriangleright \end{array} = \begin{array}{c} \blacktriangleleft \\ \blacktriangleright \end{array} = \begin{array}{c} \blacktriangleleft \\ \blacktriangleright \end{array} = \begin{array}{c} \blacktriangleleft \\ \blacktriangleright \end{array} = \begin{bmatrix} 1-\vartheta \\ \vartheta \\ -\vartheta^2 \\ \frac{1-\vartheta}{1-\vartheta} \end{bmatrix}, \quad \begin{array}{c} \blacktriangleright \\ \blacktriangleright \end{array} = \begin{bmatrix} 1 \\ 0 \\ 0 \end{bmatrix}. \quad (B.4)$$

On the other hand, the top boundary vectors act on both the auxiliary space of the MPO describing $e^{i\beta Q^{(\pm)}}$, and the auxiliary space of the fixed-point MPO, and therefore

must obtain the dependence on the charge in question and the value of β . In particular, the top boundary vector in the absence of the charge is

$$\mathbf{T} = [1 \ 1 \ 0], \quad (\text{B.5})$$

while the top boundary vector included in $\langle l_{\beta,t}^{(-)} |$ is

$$\mathbf{\Delta}^x = \mathbf{\Gamma}^x = [\delta_{x,1} \ \delta_{x,2} \ 0]. \quad (\text{B.6})$$

Unlike the bulk tensors (cf. (4.10)) the top boundary vectors of $|r_{\beta,t}^{(-)}\rangle$ are not obtained just by the flip of the sign $\beta \mapsto -\beta$, but take a completely different form,

$$x\mathbf{\Delta}^x = [1 \ \delta_{x,1} + e^{i\beta}\delta_{x,2} \ 0], \quad x\mathbf{\Gamma}^x = [1 \ \delta_{x,1} + e^{-i\beta}\delta_{x,2} \ 0]. \quad (\text{B.7})$$

We note that the overlap between the top boundary vectors of fixed-points and the boundary vectors from (3.8) reduce to the top boundary vector of the fixed-point $\langle l_t |$,

$$\mathbf{\Gamma}^x = \mathbf{\Delta}^x = \mathbf{\Delta}^x = \mathbf{\Gamma}^x = \mathbf{T}. \quad (\text{B.8})$$

In the case of $Q^{(+)}$, the top boundary vectors take the following form,

$$\begin{aligned} x\mathbf{\Delta}^x &= \begin{bmatrix} \delta_{x,1} + e^{2i\beta}\delta_{x,2} + \delta_{x,3} \\ \delta_{x,1} + \frac{e^{2i\beta}}{\gamma_+}(\delta_{x,2} + \delta_{x,3}) \\ \left(\frac{e^{3i\beta}}{\gamma_+} - 1\right)\delta_{x,1} \end{bmatrix}^T, & x\mathbf{\Gamma}^x &= \begin{bmatrix} \delta_{x,1} + e^{2i\beta}\delta_{x,2} + \delta_{x,3} \\ e^{2i\beta}\delta_{x,1} + \gamma_+(\delta_{x,2} + \delta_{x,3}) \\ (e^{3i\beta} - \gamma_+)(\delta_{x,2} + \delta_{x,3}) \end{bmatrix}^T, \\ \mathbf{\Gamma}^x &= \begin{bmatrix} \frac{e^{i\beta}}{\gamma_+}\delta_{x,1} \\ \frac{e^{2i\beta}(1-\vartheta)}{\gamma_+^2}\left(\frac{\vartheta}{1-\vartheta}\delta_{x,2} + \delta_{x,3}\right) \\ \frac{e^{2i\beta}(1-\vartheta)}{\gamma_+^2}(\delta_{x,2} - \delta_{x,3}) \end{bmatrix}^T, & \mathbf{\Delta}^x &= \begin{bmatrix} \frac{e^{i\beta}}{\gamma_+}\delta_{x,1} \\ \frac{e^{i\beta}(1-\vartheta)}{\gamma_+}\left(\delta_{x,2} + \frac{\vartheta e^{2i\beta}}{1-\vartheta}\delta_{x,3}\right) \\ \frac{e^{i\beta}(1-\vartheta)}{\gamma_+}(-\delta_{x,2} + e^{2i\beta}\delta_{x,3}) \end{bmatrix}^T, \end{aligned} \quad (\text{B.9})$$

where

$$\gamma_+ = e^{i\beta}\Lambda_{\beta}^{(+)}, \quad (\text{B.10})$$

and $\Lambda_{\beta}^{(+)}$ is given in Eq. (4.13). The two overlaps between these vectors and the boundary vectors of the $Q^{(+)}$ MPO that are needed to evaluate Eq. (5.3) are given as

$$\mathbf{\Gamma}^x = \begin{bmatrix} \frac{e^{i\beta}}{\gamma_+} \\ \frac{e^{i\beta}(1-\vartheta+e^{i\beta})}{\gamma_+^2} \\ -\frac{e^{i\beta}(1-e^{i\beta})(1-\vartheta)}{\gamma_+^2} \end{bmatrix}^T, \quad \mathbf{\Delta}^x = \begin{bmatrix} 1 \\ \gamma_+e^{-i\beta} \\ e^{2i\beta} - \gamma_+e^{-i\beta} \end{bmatrix}^T. \quad (\text{B.11})$$

Note that in the limit of $\beta \rightarrow 0$ all of the overlaps reduce to

$$\mathbf{\Delta}^x|_{\beta \rightarrow 0} = \mathbf{\Gamma}^x|_{\beta \rightarrow 0} = \mathbf{\Gamma}^x|_{\beta \rightarrow 0} = \mathbf{\Delta}^x|_{\beta \rightarrow 0} = \mathbf{T}. \quad (\text{B.12})$$

Appendix B.3. Normalization

The normalization of boundary vectors above was chosen so that the following holds,

$$\mathbf{\Delta}^x = \mathbf{\Gamma}^x = \mathbf{\Gamma}^x = \mathbf{\Delta}^x = 1, \quad (\text{B.13})$$

which together with

$$\boxed{\mathbf{\Delta}^x} = \Lambda_{\beta}^{(+)} \mathbf{\Delta}^x, \quad \boxed{\mathbf{\Gamma}^x} = \Lambda_{\beta}^{(+)} \mathbf{\Gamma}^x, \quad \boxed{\mathbf{\Gamma}^x} = \mathbf{\Delta}^x, \quad \boxed{\mathbf{\Delta}^x} = \mathbf{\Gamma}^x, \quad (\text{B.14})$$

implies

$$\langle l_{\beta,t}^{(+)} | r_{\beta,t}^{(+)} \rangle = \Lambda_{\beta}^{(+)^{2t}}, \quad \langle l_{\beta,t}^{(-)} | r_{\beta,t}^{(-)} \rangle = 1. \quad (\text{B.15})$$